









A worldwide study of subcortical shape as a marker for clinical staging in Parkinson's disease



Max A. Laansma ^{1,2,45} ✉, Yuji Zhao^{3,45}, Eva M. van Heese ^{1,2,45}, Joanna K. Bright⁴, Conor Owens-Walton ⁵, Sarah Al-Bachari^{6,7}, Tim J. Anderson ^{8,9,10}, Francesca Assogna¹¹, Tim D. van Balkom^{1,2,12}, Henk W. Berendse¹³, Fernando Cendes^{14,15}, John C. Dalrymple-Alford ^{9,16}, Ines Debove¹⁷, Michiel F. Dirx ¹⁸, Jason Druzgal¹⁹, Hedley C. A. Emsley^{20,21}, Jean-Paul Fouche²², Gaëtan Garraux ^{23,24}, Rachel P. Guimarães^{14,15}, Rick C. Helmich^{25,26}, Michele Hu²⁷, Odile A. van den Heuvel^{1,2,12}, Dmitry Isaev²⁸, Ho-Bin Kim²⁹, Johannes C. Klein ²⁷, Christine Lochner³⁰, Corey T. McMillan³¹, Tracy R. Melzer ^{8,9,16}, Benjamin Newman ¹⁹, Laura M. Parkes ^{32,33}, Clelia Pellicano¹¹, Fabrizio Piras¹¹, Toni L. Pitcher^{8,9}, Kathleen L. Poston ²⁹, Mario Rango^{34,35}, Leticia F. Ribeiro^{14,15}, Cristiane S. Rocha^{14,15}, Christian Rummel³⁶, Lucas S. R. Santos^{14,15}, Reinhold Schmidt³⁷, Petra Schwingenschuh ³⁷, Letizia Squarcina³⁸, Dan J. Stein ³⁹, Daniela Vecchio¹¹, Chris Vriend ^{1,12,40}, Jiunjie Wang^{41,42,43}, Daniel Weintraub³¹, Roland Wiest⁴⁴, Clarissa L. Yasuda ^{14,15}, Neda Jahanshad⁵, Paul M. Thompson⁵, Ysbrand D. van der Werf ^{1,2} & Boris A. Gutman³

Alterations in subcortical brain regions are linked to motor and non-motor symptoms in Parkinson's disease (PD). However, associations between clinical expression and regional morphological abnormalities of the basal ganglia, thalamus, amygdala and hippocampus are not well established. We analyzed 3D T1-weighted brain MRI and clinical data from 2525 individuals with PD and 1326 controls from 22 global sources in the ENIGMA-PD consortium. We investigated disease effects using mass univariate and multivariate models on the medial thickness of 27,120 vertices of seven bilateral subcortical structures. Shape differences were observed across all Hoehn and Yahr (HY) stages, as well as correlations with motor and cognitive symptoms. Notably, we observed incrementally thinner putamen from HY1, caudate nucleus and amygdala from HY2, hippocampus, nucleus accumbens, and thalamus from HY3, and globus pallidus from HY4–5. Subregions of the thalami were thicker in HY1 and HY2. Largely congruent patterns were associated with a longer time since diagnosis and worse motor symptoms and cognitive performance. Multivariate regression revealed patterns predictive of disease stage. These cross-sectional findings provide new insights into PD subcortical degeneration by demonstrating patterns of disease stage-specific morphology, largely consistent with ongoing degeneration.

Alterations in subcortical brain regions play a crucial role in a wide range of clinical domains known to be affected in Parkinson's disease (PD), including motor, cognitive, emotional, and autonomic functioning¹. It remains to be fully elucidated, however, how and to what extent localized morphological differences in the basal ganglia, thalamus, amygdala, and hippocampus contribute to the clinical manifestation of PD in vivo.

Shape analysis quantifies local inward and outward variations of the gray matter surface boundaries, complementing standard global volumetry as it can identify subtle regional differences that may not affect total volume. Considering the complex organization of subcortical brain regions, with each nucleus consisting of functionally specialized subdivisions, subcortical shape analysis can provide insights into local vulnerability to disease. An

overview of prior findings using shape analysis to study PD is provided in Table S1 in Supplement²⁵. The majority of case-control studies reported subregional alterations of the putamen and caudate nucleus in PD^{2,4,5,8,12,23,25}, while several studies also demonstrated shape abnormalities in the globus pallidus^{3,6,12}, hippocampus^{6,8}, nucleus accumbens⁷, and thalamus^{7,12,19}. The use of predictive modeling to distinguish PD patients from controls based on shape features has been explored; predictive modeling applications in smaller datasets have shown moderate to high classification performance^{3,20,21,24}.

While these findings show promise, the reported effects across studies in terms of location, direction, and size vary substantially, which hampers a clear understanding of disease patterns. The inconsistencies may be partly explained by the small sample sizes of individual studies, differences between study sample characteristics, the method quantifying morphometric shape, and the regions of interest selected. Machine learning studies in particular are highly susceptible to overfitting²⁶. To address these limitations, it is essential to conduct a well-powered study on a large PD sample that transcends geographical and cultural boundaries, utilizing harmonized processing methods.

Here we present findings from the largest international collaborative analysis of subcortical shape in PD to date, using a combination of mass univariate group comparisons, correlations, and interpretable machine-learning approaches. We aimed to elucidate region-specific morphology patterns and associations with clinical measures. We intended to apply predictive models, not to reach high classification for diagnostic purposes, but rather to better understand disease-stage-related patterns of morphology using a multivariate approach, expanding on our previous work detailing global subcortical volumetry in PD²⁷. In line with our prior work, we expected overall thinner subcortical regions in PD compared to controls, except for increased thalamic thickness in mild stages of the disease²⁷.

Results

Full sample

Data flow for each analysis is depicted in Fig. S1 and a summary of demographic and clinical measures for the PD and control group per source is provided in Table 1 and per cohort in Table S2 in the Supplement. There was a significant difference in age ($D = 0.12$, $p < 0.001$) and sex ($\chi^2(1, n = 3851) = 39.3$, $p < 0.001$) between the PD and control group.

Mass univariate analysis: case-control

The majority of structures were regionally thinner in PD, with the largest differences in the putamen ([% significant of all vertices, peak beta value] left: 42.3%, -0.17 ; right: 49.2%, -0.18). The thalami, caudate nuclei, globus pallidus, putamen, and left amygdala were regionally thicker, with the largest differences in the thalami (left: 32.4%, 0.13; right: 32.4%, 0.13; Fig. 1A–D and Tables S3 and S4 in the Supplement). A comparison of age- and sex-matched PD ($n = 2502$, 35% female, age 63.5 ± 9.5 years) and control ($n = 610$) subsample overall aligned with these patterns (Fig. S2A–B in the Supplement).

Mass univariate analysis: HY stages

A summary of demographic and clinical measures across Hoehn and Yahr (HY) stages is depicted in Table S5 in the Supplement. Mann–Whitney tests revealed significant differences in the time since diagnosis and Montreal Cognitive Assessment (MoCA) score among all HY groups (Fig. S3A, B in the Supplement). The matching procedure selected 887 controls to match the 451 HY1 participants, 1068 controls to match the 1068 HY2 participants, 846 controls to match the 282 HY3 participants, and 680 controls to match the 85 HY45 participants. The control sample partially overlapped across stage analyses (Table S6 in the Supplement). For optimal matching, some HY2 (135), HY3 (1), and HY45 (1) participants were removed from this analysis.

Case-control shape differences were found for all HY stages, notably showing thinner putamen in HY1 ([% significant of all vertices, peak beta value] right: 8.2%, -0.18) and HY2 (left: 16.5%, -0.14 ; right: 21.8%, -0.17)

and thicker bilateral thalamus in HY1 (left: 8.9%, 0.19; right: 19.5%, 0.13) and HY2 (left: 10.5%, 0.15; right: 19.5%, 0.13). Thinner subregions of all structures were identified in HY3 and HY45 (Fig. 2A–D and Table S7A–D in the Supplement). Excluding age and sex as covariates to the models generated comparable patterns (Fig. S2C–F in the Supplement).

Spin permutation tests revealed significant similarities in disease patterns, with breaks in similarity generally between HY2 and HY45. HY1 and HY2 maps were significantly similar for the right putamen (spatial correlation coefficient $r = 0.52$, $p < 0.001$), right caudate nucleus ($r = 0.48$, $p < 0.001$), left globus pallidus ($r = 0.19$, $p = 0.016$), right nucleus accumbens ($r = 0.53$, $p = 0.006$), and thalamus bilaterally (left: $r = 0.46$, $p < 0.001$; right: $r = 0.39$, $p < 0.001$). HY2 and HY3 maps were similar bilaterally for the putamen (left: $r = 0.53$, $p < 0.001$; right: $r = 0.62$, $p < 0.001$) and caudate nucleus (left: $r = 0.60$, $p < 0.001$; right: $r = 0.28$, $p < 0.001$) and the left thalamus ($r = 0.26$, $p = 0.004$). HY3 and HY45 maps were similar for all ROIs ($r_{\min} = 0.46$; $r_{\max} = 0.93$) except the globus pallidus bilaterally and the left thalamus (see Fig. S4A–C).

Mass univariate analysis: time since diagnosis, MoCA, and MDS-UPDRS3

A subsample of PD participants had time since diagnosis ($n = 2350$), MoCA ($n = 1216$), and Movement Disorder Society-sponsored revision of the Unified Parkinson's Disease Rating Scale part 3 (MDS-UPDRS3) ($n = 1153$) scores available. Demographic and clinical characteristics of these subsets are provided in Table S8 in the Supplement. All three variables were moderately correlated with each other (Table S9 in the Supplement).

Increasing time since diagnosis was associated with regional thinning in the putamen, caudate nucleus, amygdala, and nucleus accumbens, and to a lesser extent in the thalamus and hippocampus (Fig. 3A and Table S10 in the Supplement). Worse MoCA performance was predominantly associated with regional thinning in the bilateral putamen, amygdala, caudate nucleus, nucleus accumbens, and hippocampus, as well as thicker subregions in the bilateral caudate nucleus, right globus pallidus, and right thalamus (Fig. 3B and Table S11 in the Supplement). Worse MDS-UPDRS3 performance was predominantly associated with regional thinning of the bilateral thalamus, amygdala caudate nucleus, and left nucleus accumbens, as well as thicker subregions of the bilateral caudate nucleus and globus pallidus (Fig. 3C and Table S12 in the Supplement).

Predictive models for HY classification

The patterns of expansion and contraction in the binary classification largely correspond to the patterns shown in the mass univariate model (Fig. 4A), while the ordinal classification shows more dispersed patterns of contractions and expansions (Fig. 4B). Overlaying a hippocampal subfield atlas over the ordinal shape patterns showed greatest atrophy in CA1, CA3, and regions surrounding the hippocampal fissure, and relative sparing of the fimbria and subiculum (Fig. S5A, B in the Supplement).

The TV-L1 regularized logistic regression (Logit-TVL1) model achieved a receiver operating characteristic area-under-the-curve (ROC-AUC) score of 0.65 for the full PD sample compared to controls, 0.61 for HY1 vs HY2 and 0.66 for HY2 vs HY345 classification. The binary classification maps of HY stages contrasted with each other and controls are shown in Figs. S6A–C, S7A–C, and S8A–C in the Supplement. We report on the classification performance between the multi-task classification models (one-against-all vs ordinal logistic regression (Ordit) model) in Table S13 and Fig. S9A–E in the supplement. Additional validity checks on the caudate nucleus revealed no differences in medial curve discrepancy between sites, the PD and control group, and HY disease stages (Fig. S10A–D).

Discussion

In the largest study on subcortical shape in PD to date, we found local abnormalities of subcortical brain regions in people with PD compared to controls across all disease stages. Each HY increment was characterized by greater impairment in both cognitive and motor domains, as well as greater time since diagnosis, on average, highlighting the close relationship between

Table 1 | Demographics complete sample

Site	N cohorts	N	N females			Age ± SD			Time since diagnosis ± SD			MoCA ± SD			MDS-UPDRS3 OFF ± SD		
			All, (%)	HC	PD	HC	PD	HC	PD	HC	PD	HC	PD	HC	PD	HC	PD
Amsterdam	3	295 (7.7)	74	221	29	29	58.97 ± 9.95	63.17 ± 9.59	NA	3.58 ± 3.95	28.23 ± 1.48	26.20 ± 2.17	NA	28.59 ± 12.74			
Bern	2	106 (2.8)	51	55	27	29	62.45 ± 9.92	62.76 ± 10.19	NA	12.36 ± 4.42	NA	23.00 ± 5.66	NA	39.56 ± 12.90			
Campinas	1	240 (6.2)	132	108	81	36	58.88 ± 7.77	59.84 ± 10.27	NA	7.33 ± 6.44	NA	NA	NA	NA			
Cape Town	1	17 (0.4)	7	10	3	2	66.57 ± 5.68	66.30 ± 5.91	NA	7.12 ± 3.68	26.29 ± 1.89	25.60 ± 3.50	NA	NA			
Chang Gung	1	550 (14)	223	327	120	139	60.95 ± 7.28	60.09 ± 9.63	NA	8.70 ± 6.33	NA	NA	NA	28.19 ± 16.93			
Charlottesville	3	179 (4.6)	179	179	NA	45	NA	64.31 ± 8.87	NA	9.25 ± 4.62	NA	24.54 ± 3.63	NA	37.19 ± 10.69			
Christchurch	1	263 (6.8)	53	210	18	56	69.13 ± 8.14	69.45 ± 7.77	NA	5.77 ± 5.59	27.06 ± 2.13	23.58 ± 4.18	NA	31.15 ± 17.35			
Donders	1	82 (2.1)	23	59	11	26	62.65 ± 10.29	60.81 ± 10.07	NA	4.42 ± 3.79	NA	NA	NA	32.98 ± 15.63			
Graz	2	250 (6.5)	125	125	34	34	63.58 ± 10.17	63.58 ± 10.15	NA	4.60 ± 4.98	NA	NA	NA	28.60 ± 19.28			
Liege	2	151 (3.9)	76	75	36	31	65.26 ± 6.85	66.48 ± 7.60	NA	6.47 ± 4.55	NA	NA	NA	17.67 ± 9.87			
Milan	1	73 (1.9)	25	48	15	15	53.48 ± 8.80	57.54 ± 7.53	NA	11.09 ± 3.55	NA	NA	NA	27.40 ± 11.23			
Neurocon ^a	1	42 (1.1)	15	27	12	10	66.73 ± 11.74	68.70 ± 10.55	NA	NA	NA	NA	NA	28.33 ± 9.27			
NW-England	2	89 (2.3)	43	46	19	10	68.79 ± 7.29	68.43 ± 8.08	NA	7.55 ± 5.01	27.63 ± 2.19	25.23 ± 3.95	NA	NA			
ON Japan ^a	1	45 (1.2)	15	30	8	17	63.33 ± 5.25	67.57 ± 6.81	NA	NA	NA	NA	NA	NA			
Oxford	1	181 (4.7)	66	115	23	41	65.95 ± 8.67	63.96 ± 10.17	NA	2.29 ± 1.58	27.36 ± 2.04	26.39 ± 2.79	NA	28.56 ± 13.69			
Pennsylvania	1	122 (3.2)	11	111	6	35	70.09 ± 5.86	66.45 ± 7.87	NA	7.35 ± 5.48	NA	25.50 ± 3.30	NA	NA			
PPMI ^b	21	504 (13)	159	345	58	120	60.40 ± 11.45	61.67 ± 9.67	NA	0.58 ± 0.56	28.26 ± 1.11	27.15 ± 2.26	NA	20.29 ± 8.59			
Rome SLF	1	367 (9.5)	127	240	51	88	36.61 ± 10.56	62.90 ± 10.15	NA	4.96 ± 4.15	NA	NA	NA	16.67 ± 10.67			
Stanford	2	213 (5.5)	63	150	39	61	65.53 ± 8.42	68.14 ± 8.68	NA	5.26 ± 4.02	26.95 ± 2.03	25.60 ± 4.27	NA	34.86 ± 12.20			
Tao Wu ^a	1	39 (1.0)	20	19	8	9	64.75 ± 5.58	65.00 ± 4.45	NA	5.32 ± 4.00	NA	NA	NA	NA			
Udall ^a	1	43 (1.1)	18	25	11	7	62.55 ± 9.97	66.15 ± 10.00	NA	8.93 ± 4.86	27.83 ± 1.47	26.40 ± 2.12	NA	NA			
Total	50	3851	1326	2525	609 (35%)	896 (46%)	60.00 ± 12.20	63.69 ± 9.75	NA	5.59 ± 5.43	27.72 ± 1.78	25.69 ± 3.52	NA	28.25 ± 14.39			

N sample size, sd standard deviation, MoCA Montreal Cognitive Assessment, MDS-UPDRS3 Movement Disorders Society sponsored revision of the Unified Parkinson's Disease Rating Scale part 3, HC healthy controls, PD Parkinson's disease.

^aOpen dataset.

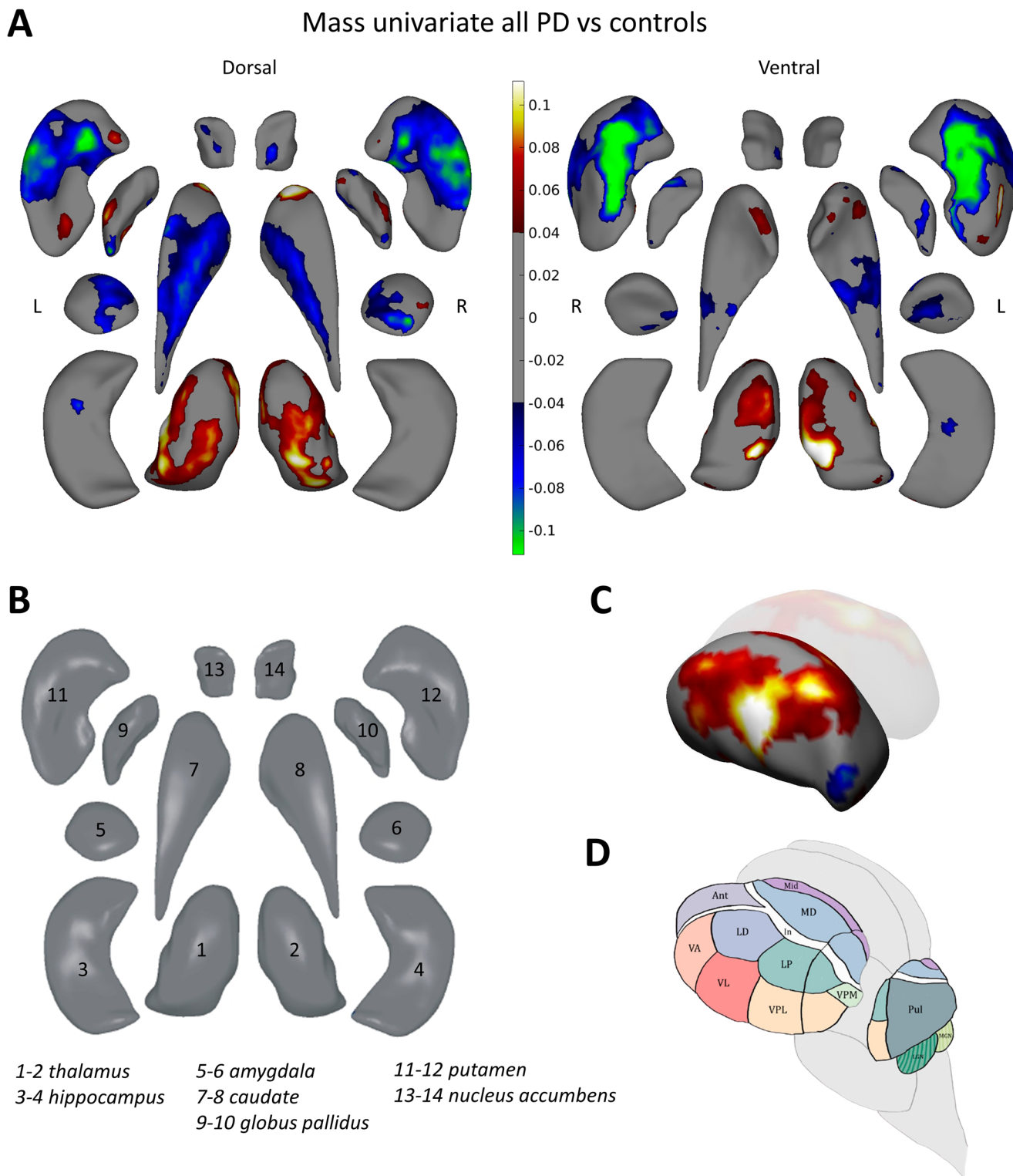


Fig. 1 | Mass univariate analysis: significant vertex-wise differences in thickness between the full PD group and controls. **A** Effect map projected onto the subcortical regions showing the PD versus control group comparison. Positive b -values indicate that regions are thicker and negative b -values indicate that regions are thinner in PD compared to controls. The model is corrected for age, sex, intracranial volume and cohort. **B** A dissection of the fourteen subcortical structures of interest in this study to guide the interpretation of panel (A). **C** Thalamus effect maps showing

group differences and **D** anatomical drawing of the thalamus and its subnuclei displayed approximately in the same angle for interpretation purposes. L left hemisphere, R right hemisphere, Ant anterior nucleus, In intralaminar nuclei, LD lateral dorsal nucleus, LGN lateral geniculate nucleus, LP lateral posterior nucleus, MD mediodorsal nucleus, MGN medial geniculate nucleus, Mid midline nuclei, Pul pulvinar nucleus, VA ventral anterior nucleus, VL ventral lateral nucleus, VPL ventral posterior lateral nucleus, VPM ventral posterior medial nucleus.

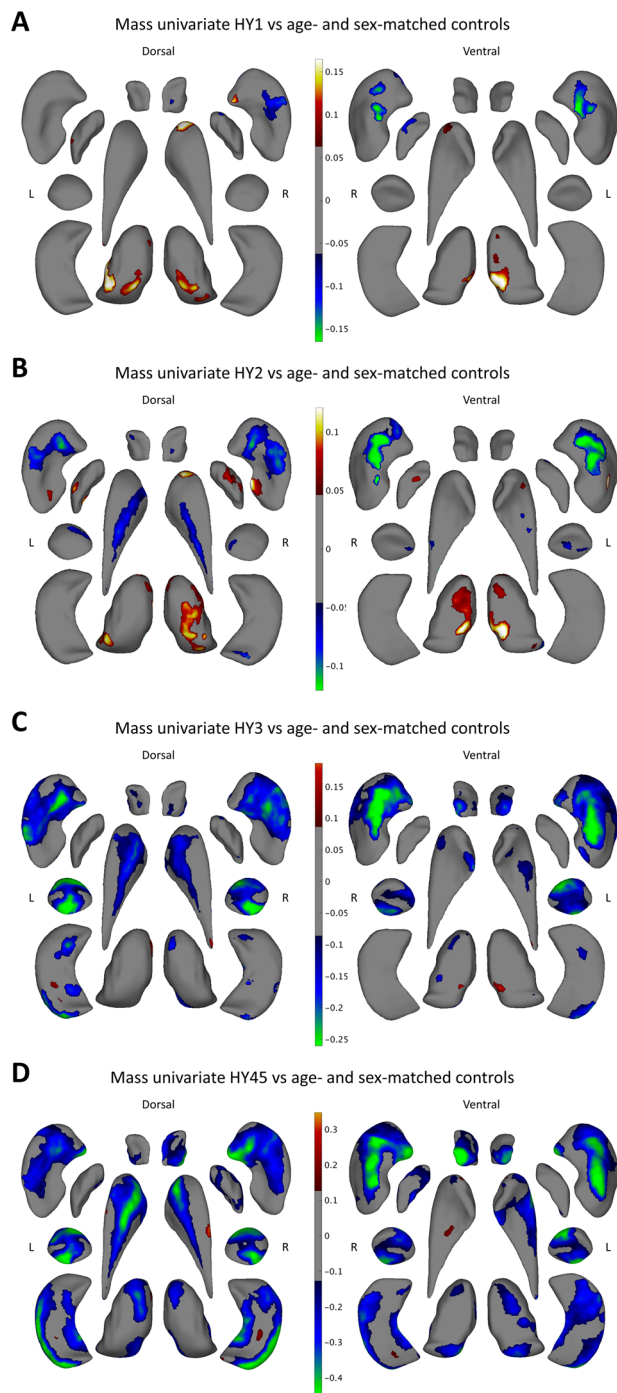


Fig. 2 | Mass univariate analysis: significant vertex-wise differences in thickness between HY stage and age- and sex-matched controls. A HY1, B HY2, C HY3, and D HY45 results are shown in the dorsal and ventral view. Positive b -values indicate that regions are thicker in the PD group compared to controls and negative b -values indicate that regions are thinner. The models are corrected for intracranial volume, age, sex, and cohort. HY Hoehn and Yahr.

HY staging and overall clinical progression²⁸. Accordingly, the cross-sectional HY stage patterns are in line with the neurodegenerative process that is expected in PD, suggesting progressive thinning of selective subregions of the basal ganglia and limbic regions. This overall aligns with longitudinal findings in mild to more severe PD stages showing the most marked atrophy in the striatum and amygdala²⁹.

Largely symmetrical and focal patterns of abnormal shape were found in low stage PD, and more diffuse and pronounced across all structures in

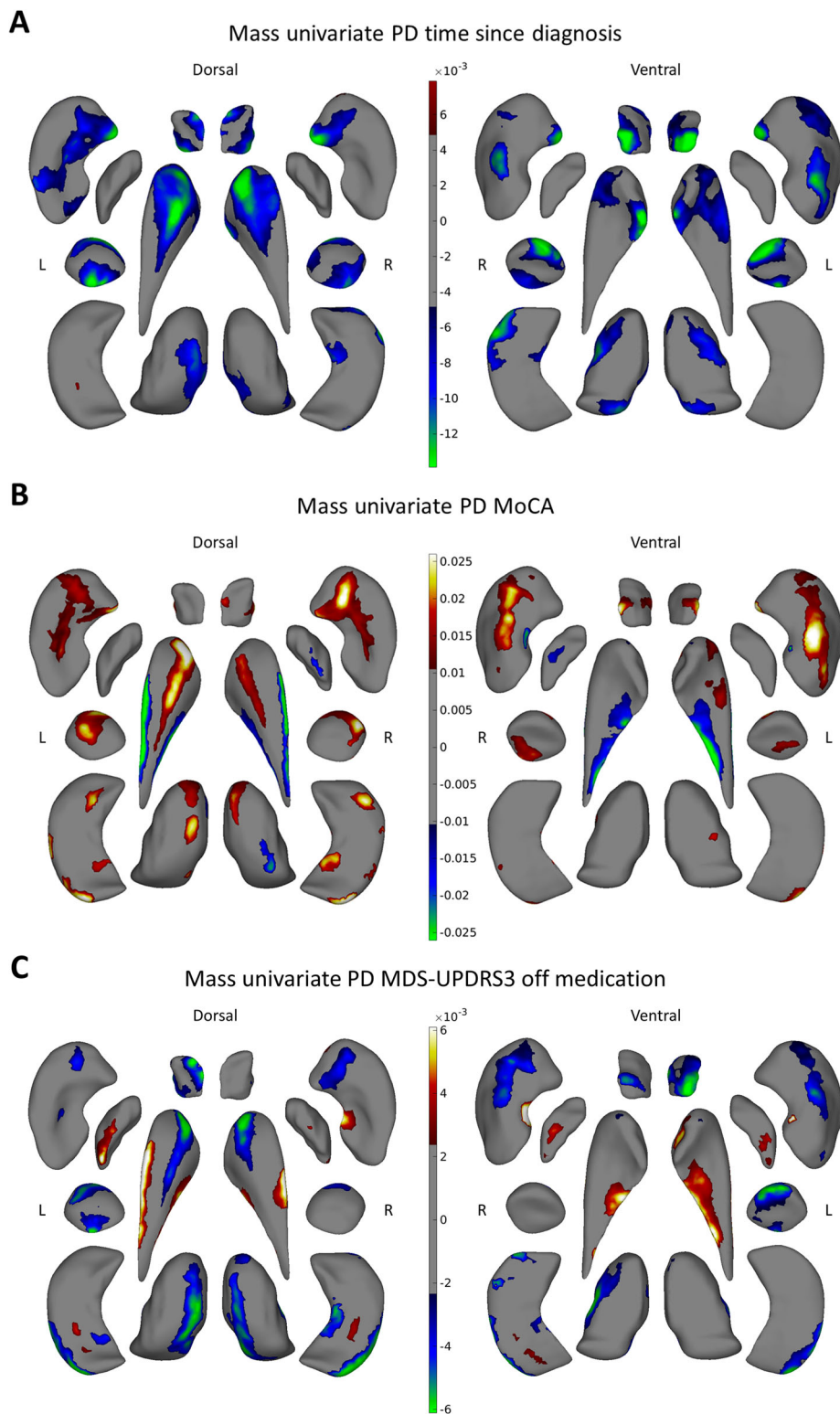
higher disease stages. Notably, relatively thinner striatal regions can be observed at the lowest stages. This includes parts of the medial putamen, followed by posterior and anterior putamen regions, and parts of the dorsal caudate nucleus. Later HY stage associations involve the ventral striatum, including the nucleus accumbens. Of note is that the staging pattern aligns with the framework describing the deterioration of the nigrostriatal pathway in PD; subregions of the striatum are shown to not be equally and simultaneously affected; rather, evidence suggests a systematic distribution of pathology across striatal subfields with disease progression, in a similar pattern as presented in the current study^{30–34}. Conjecturally, spatial similarity analysis across HY stages suggests that a substantial change in the morphometric correlates of PD progression takes place between HY2 and HY3 across nearly all subcortical regions considered. Only the globus pallidus and the left thalamus have consistent differential patterns of atrophy from HY1 through HY3, with only the HY45-associated shape effects being different from effects in earlier stages.

Cognitive impairment and dementia become increasingly frequent as PD progresses³⁵. The implication of first the amygdala and then the hippocampus, accompanied by more selective anterior putamen and anterior-medial dorsal thalamus involvement, fit the expected decline in cognition in this group^{30,36}, further emphasized by overlapping subregions that were associated with lower cognitive performance. Overall, the demonstrated regional thinning associated with a longer time since diagnosis agrees with the patterns found in the staging analysis, with a notable difference: the non-linear and non-uniform thalamic pattern across stages can not be captured by the linear regression model, while in turn the implicated subregions largely align with the final HY stage. Regions showing thinning associated with global cognitive and motor impairment largely overlap, highlighting the congruent progression of both domains in PD overall³⁷. The bidirectional patterns in the caudate nucleus suggest that the progression of motor and cognitive symptoms is associated with complex shape changes.

Few regions, including parts of the medial dorsal and (ventral) posterolateral thalamus, head of the right caudate nucleus, and lateral globus pallidus, were thicker in mild-stage PD, and did not exhibit thinning even in higher stages. This would suggest that distinct subregions may be temporarily enlarged and then normalized during the disease process, or may be larger pre-morbidly. The clustering of the mild-stage participants based on shared thalamic shape features revealed no distinct clinical profiles of the identified clusters, suggesting that the variation in thalamic size is not explained by global motor or cognitive severity, see Fig. S11 and Table S14A–D. Possibly, more specific symptom domains are associated with focal enlargement. There is supporting evidence that thalamic hypertrophy may occur in early PD³⁸, and could possibly be linked to increased connectivity of thalamic subdivisions that are involved in basal ganglia-thalamocortical and cerebellothalamic circuitry responsible for controlling movement, including the ventral anterior and ventral lateral territories, respectively^{39,40}. Evidence suggests that increased functional connectivity of the globus pallidus interna and putamen with the cerebellothalamic pathway is likely involved in the pathophysiology of PD tremor³⁹. The continuous activation of the motor system in PD, as well as compensatory homeostasis by remaining cells, may result in a temporary increase in tissue size; a model supported by observations that depletion of striatal dopamine is associated with both striatopallidal hyperactivity⁴¹ and enlargements of striatopallidal synaptic boutons⁴². The demonstrated relation between greater motor impairment and selectively thicker putamen, caudate nucleus, and globus pallidus territories in this study, and similar findings from a recent study⁴³, further support this notion. Other thalamic subdivisions that are among the most densely innervated by dopamine, including the midline limbic nuclei and mediodorsal and lateral posterior association nuclei⁴⁴, seem to be predominantly implicated in mild PD. The pattern agrees with histopathological studies showing that the largest concentrations of Lewy body pathology are found in limbic territories of the thalamus, with the sensory-motor subdivisions being relatively spared^{45,46}.

The difference in model maps between binary classification and ordinal HY staging suggests that the morphometric correlates of PD do not

Fig. 3 | Mass univariate analysis: significant vertex-wise correlation between clinical measures and thickness within the PD group. **A** Time since diagnosis, **B** MoCA, and **C** MDS-UPDRS3 motor score while off medication are shown. Positive *b*-values indicate a positive correlation and negative *b*-values indicate a negative correlation. All regression analyses were corrected for age, sex, and intracranial volume. MoCA Montreal cognitive assessment, MDS-UPDRS3 OFF Movement Disorders Society-sponsored revision of the Unified Parkinson's disease rating scale part 3 assessed in OFF medication state.



vary linearly with disease progression. While regions such as the dorsal caudate nucleus and medial putamen are consistently important in disease prediction, other regions have a more nuanced course. In particular, the dorsal thalamic subregion sees initial expansion (consistent with the univariate analysis), followed by compression in the Ordit model (which excluded control participants). While the binary and ordinal models both work by producing simple linear combinations of local morphometric features, the ordinal model allows for this linear combination to be related non-linearly to a granular measure of disease severity with the addition of

only a few more parameters. Critically, this way Ordit strikes a balance between anatomical interpretability and accuracy in severity prediction.

In contrast to univariate analysis, a negatively-weighted region of a subcortical boundary in Ordit may not necessarily imply focal atrophy. While such an interpretation may well be correct, it is also possible that such a region experiences an expansion that is highly correlated with, but reduced relative to, another region with more marked gray matter contraction. In this sense, multivariate maps must be observed as a whole rather than the sum of individual parts⁴⁷. It is precisely this “whole-picture” representation

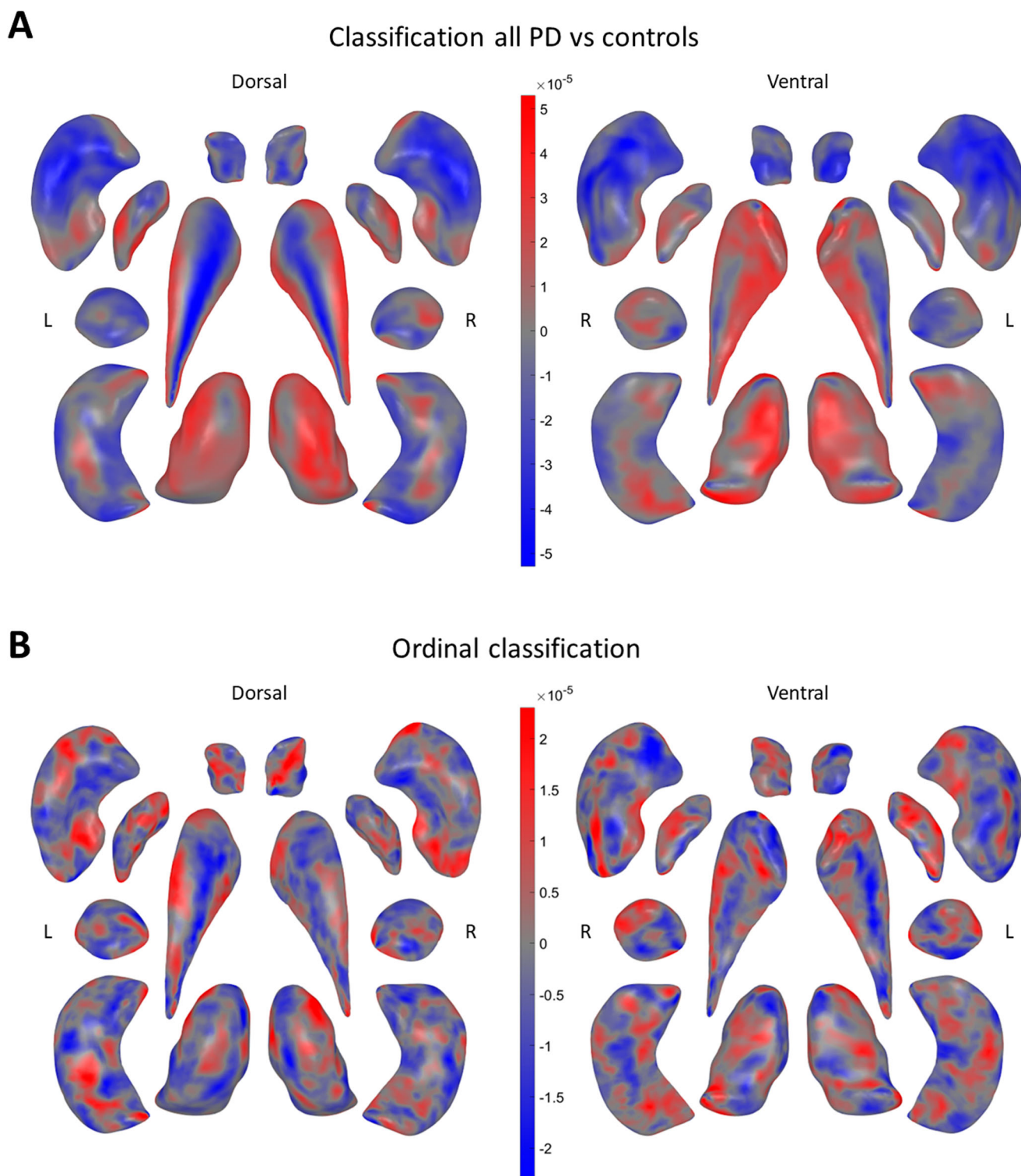


Fig. 4 | Machine learning: binary and ordinal classification maps. Binary and ordinal classification uses vertex-wise thickness information from all subcortical structures. The color bars represent the learned weights of the classification model, positive values (SD from the learned weights) in red, and negative values in blue.

More intense colors indicate a stronger predictive power of the classification. Displayed are the results of **A** the binary classification of people with PD and controls, **B** the ordinal classification of HY1–HY2–HY345.

of disease effects—rather than the power to make diagnostic predictions—that captures the value of a multivariate linear shape classifier in the context of PD imaging.

A number of limitations should be discussed. First, the cross-sectional nature of this study complicates making inferences on disease progression.

In spite of this, it is striking that the morphometric and clinical patterns in separate PD groups are correlated and strongly incremental, in agreement with progressive degeneration. Secondly, subsamples were available for the analysis due to missing data for some cohorts. While we are aware this may challenge the exchangeability of findings between analyses, we emphasize

the unprecedentedly large samples that remained available, enabling the detection of subtle disease patterns that can not be adequately assessed in smaller, underpowered studies. Thirdly, the number of available participants across HY stages was imbalanced. The fewer participants in HY4 and HY5 necessitated combining participants at stage HY3 and higher into one group for the purposes of ordinal regression. This is, however, mitigated by the clinical intuition that the greatest qualitative jump in symptom severity occurs between HY2 and HY3. Fourthly, the level of striatal morphometric asymmetry is possibly dependent on body asymmetry of motor symptom severity, more pronounced in early than late PD stages⁴⁸, which we could not investigate here, but aim to include in future analyses. Finally, the shape method provides fine-grained information on surface deformations, but it does not capture the underlying structure. This reduces the translatability to the subnucleus level, especially in structurally complex brain regions such as the thalamus.

The findings of this unprecedented large study offer new insights into patterns of subcortical degeneration and associations with symptom domains in PD. Notably, the relation between clinical staging and shape alterations aligns with the progressive nature of PD.

Methods

Participants

The data in this study were acquired between September 2016 and January 2022 and subsequently pooled by the ENIGMA-PD working group. A total of 3851 3D T1-weighted brain MR images, of 2525 individuals with PD (35% female, age 63.69 ± 9.75 years [mean \pm SD]) and 1326 control participants (46% female, 60.00 ± 12.20 years), were included from 22 different sources, resulting in 50 cohorts with distinct scanning and clinical testing environments (Fig. S12). MR images were collected and processed by the individual source institutions; the output of the processing pipeline was uploaded to a central repository for statistical analysis. Clinical characteristics such as HY stage⁴⁹, time since diagnosis, MoCA scores⁵⁰, and scores from the UPDRS⁵¹ and the MDS-UPDRS⁵² obtained in the OFF state were requested for all PD participants and, if available, for controls. HY stage was used as a measure of disease severity and ranged from HY1 to HY5. Participants who were allocated to stages HY1.5 or HY2.5, according to the modified HY classification, were regrouped into HY2. Similarly, smaller groups of PD participants with the most severe stages were merged to increase statistical power, resulting in HY45 for mass univariate analyses and HY345 for the machine learning experiments. Nearest neighbor-matching using the *MatchIt* package in R was performed to create subsamples of age- and sex-matched controls for each HY PD group⁵³. Cohort-specific inclusion and exclusion criteria are summarized in Table S2 in the Supplement.

Imaging acquisition and subcortical shape analysis

T1-weighted MRI scans were collected according to local MRI protocols (Table S15 in the Supplement). All scans were processed using the automated ENIGMA-shape pipeline including FreeSurfer v5.3 recon-all and subcortical parcellation tools^{54–59}, together with Matlab and R scripts to perform statistical analysis and visualization (<http://enigma.ini.usc.edu/ongoing/enigma-shape-analysis>)^{60,61}. For each participant, the pipeline extracted a surface mesh of seven regions of interest (thalamus, caudate nucleus, putamen, globus pallidus, hippocampus, amygdala, and nucleus accumbens, unilaterally) representing the outer boundaries of the region. A measure of radial distance was used to examine regional shape deformations across participants, which is computed as the distance from the surface to the medial curve, a smooth curve that is fitted through the approximate center of each structure. This distance is further referred to as thickness^{60,62}. Detailed steps of the ENIGMA-Shape pipeline (Fig. S13) and a second measure of shape morphometry (Figs. S13, S14A–H, and S15A–C and Table S16A–H) are reported in the Supplement.

Mass univariate statistics

Mass univariate statistics across vertices were computed using the *lme4* package with standardized R scripts⁶³. Vertex-wise group differences (full

sample and HY stages vs controls) in thickness were assessed using linear mixed-effects models with the variable *cohort* as a random intercept. Age, sex, and total intracranial volume were added as nuisance covariates. We additionally tested vertex-wise correlations between thickness and variables time since diagnosis (in years), MoCA score, and (MDS-)UPDRS3 off-medication score. UPDRS3 scores were converted to MDS-UPDRS3 scores using a validated formula⁶⁴. For each vertex, we corrected the *p*-value from the mass univariate analyses for multiple comparisons using searchlight false discovery rate correction, at $q = 0.05$ as further explained in the legend of Fig. S13⁶⁵.

Permutation tests

Over the course of this study, several related statistical maps were derived modeling disease effects at different stages on deep gray-matter structures. The abundance of spatially distributed statistical tests naturally begs the question: in what ways are the patterns of disease similar over the course of PD progression? To quantify spatial coherence between two different effects, we adapted a previously established approach in neuroimaging known as the “spin test”⁶⁶. Briefly, the idea is to preserve the overall spatial structure of the effect pattern while randomly shifting the pattern position with respect to the other effect in the pair. In this way, we can bootstrap a null distribution of spatial correlations between two effect maps—independently in any given brain region—and compare it to the observed correlation. In the case where effects are mapped to a surface of spherical topology, the shift can be accomplished by a spherical rotation leading to the term “spin test”. Here, we generated 10,000 random rotations for each test, using a quaternion representation. The strength of evidence that the patterns are indeed correlated more strongly than by chance can then be measured in the usual frequentist way: the *p*-value is the proportion of times that the absolute value of the observed correlation is greater than the absolute value of the null distribution draws.

Multivariate predictive models

Due to the unfavorable sample-to-feature ratio in neuroimaging data, effective regularization is critical to train interpretable models that generalize well outside of the training samples. Here, we used a logistic regression (logit) model with “Structured Sparsity”, in which the linear vertex loadings are sparse (using the “L1” norm) and spatially cohesive (using the “Total Variation” or “TV” norm). This combination has been shown to substantially improve model interpretability⁶⁷. Logit-TVL1 has been widely used in functional and diffusion MR brain imaging^{67,68}, and more recently for regression and spectral analysis of mesh-based data⁶⁹.

The case-control binary classification was performed by training the Logit-TVL1 on vertex-wise thickness across all structures. Hyper-parameters weighing the relative importance of the TV and L1 terms were optimized using a grid search with 4-fold cross-validation (CV). For assessment, ROC-AUC scores were computed using a “nested” 4-fold-CV approach, which eliminated much of the uncertainty resulting from selecting a single random independent validation subset. Our methods for imputation of missing data and accounting imbalanced groups are described in the legend of Fig. S13.

To identify a multivariate signature of disease progression across all stages using HY stages as the target variable, we used the natural extension of the Logit classification, the Ordit. Briefly, Ordit models consider HY stages to be ordered without assuming any specific functional relationship—such as a linear dependence—between stage and biomarker value. The task is then to simultaneously identify a universal linear multivariate stage progression model and $K - 1$ thresholds $\theta_1 < \theta_2 < \theta_3 < \dots < \theta_{K-1}$, where K is the number of stages considered. As with the binary models, we used Structured Sparsity regularization. We applied our ordinal classifier using three HY stage classes (HY1, HY2, and HY345). We followed the same hyperparameter tuning and cross-validation approach as with binary classifiers, replacing AUC with a balanced F1 score as performance criteria.

Inclusion and ethics statement

Within the PD working group of the ENIGMA consortium, we strive for inclusivity by allowing researchers from around the globe to participate in

large-scale and impactful investigations. We actively encourage participation from low-income countries and aim to uncover biological insights that transcend borders, race, and socioeconomic status differences. This research was conducted in accordance with the World Medical Association's Declaration of Helsinki. Approval from the respective institutional review boards and written consent from participants were obtained at each source institution: Amsterdam—Amsterdam I: Medisch Ethische Toetsingscommissie VU Medisch Centrum approval #ID2018.198. Amsterdam II: COGTIPS, METc VUmc #NL58750.029.16 (2016.543). Amsterdam III: Medisch Ethische Toetsingscommissie VU Medisch Centrum approval #ID2018.198. Bern—BE I–II: approved by the Cantonal Ethics Committee (CEC) #2016-00369. Cape Town—Cape Town Stellenbosch: approved by IRBs at Stellenbosch University (IRB reference number: M07/05/019) and the University of Cape Town (IRB reference number: 261/2007). Chang Gung—CGU: Chang Gung Medical Foundation Institutional Review Board #202001592B0. Charlottesville—Charlottesville I–III: University of Virginia Institutional Review Board for Health Science Research #16778. Christchurch: Southern Health and Disability Ethics Committee of the New Zealand Ministry of Health #URB/09/08/037/AM07. Donders—Donders Radboud: METC Oost-Nederland #2014-123 and CMO Regio Arnhem, Nijmegen NL47614.091.14. METC 2014/014. Liege—Liege I–II: The Ethics Committee of the University of Liège approved the study. <https://www.sciencedirect.com/science/article/pii/S1053811914005102>. Milan: Fondazione Ca' Granda, IRCCS, Policlinico, the ethical committee approved, authorization granted by Dr. Giuseppe Di Benedetto, General Director, dated November 19, 2008. This authorization is issued under the authority of Legislative Decree 211/2003, Article 2, Paragraph 1." Determination number: n.172. NW-England—NW-England I–II: NWE, ethics (North West—Preston Research Ethics Committee) IRAS ID #122770 REC reference 13/NW/0295. Oxford—Oxford DISCOVERY: South-Central Oxford Research Ethics Committee #15/SC/0117. Pennsylvania: University of Pennsylvania Institutional Review Board Protocol #820710. Graz—PROMOVE ASPS I–II: Ethics Committee of the Medical University of Graz #21-345-ex 09/10 and IRB: Medical University of Graz PROMOVE 21-345 ex 09/10 ASPSF: 17-088 ex 05/06. Rome—Rome SLF: Fondazione Santa Lucia Local Institutional Review Board. Approval ID #CE/PROG.905. Stanford—Stanford I–II: The MJFF MRI study (IRB-22722) and the ADRC study (IRB-33727). Campinas—UNICAMP: Comitê de Ética de Pesquisa da UNICAMP; approval #CAAE: 45873415.9.0000.5404.

Data availability

Publicly available datasets used in this work include PPMI (ppmi-info.org), OpenNeuro Japan including Udall cohort (openneuro.org/datasets/ds000245/), and Neurocon and Tao Wu's data set (icon_1000.projects.nitrc.org/indi/retro/parkinsons.html). Individual ENIGMA-PD sites retain ownership of their MRI scans and only share the anonymized derived data for this analysis. Data are thus not openly available, but researchers are invited to join the ENIGMA-PD Working Group where they can formally request derived data via secondary proposals. Data requests are then considered by the individual site's principal investigators. If you are interested in joining ENIGMA-PD, please contact enigma-pd@amsterdamumc.nl. For more information please see the working group website: <https://enigma.ini.usc.edu/ongoing/enigma-parkinsons/>.

Code availability

The ENIGMA-Shape pipeline with code to perform processing, statistical analysis, and visualization is available here: <http://enigma.ini.usc.edu/ongoing/enigma-shape-analysis>. The source code for the in-house analysis scripts for the predictive modeling analysis is made available here: <https://github.com/LAMCIG/ML-for-surface-data>.

Received: 13 May 2024; Accepted: 21 October 2024;
Published online: 19 November 2024

References

1. Draoui, A., El Hiba, O., Aimrane, A., El Khat, A. & Gamrani, H. Parkinson's disease: from bench to bedside. *Rev. Neurol.* **176**, 543–559 (2020).
2. Nemmi, F., Sabatini, U., Rascol, O. & Péran, P. Parkinson's disease and local atrophy in subcortical nuclei: insight from shape analysis. *Neurobiol. Aging* **36**, 424–433 (2015).
3. Menke, R. A. L. & Szewczyk-Krolikowski, K. Comprehensive morphometry of subcortical grey matter structures in early-stage Parkinson's disease. *Hum. Brain Mapp.* **35**, 1681–1690 (2014).
4. Lee, H. M. et al. Subcortical grey matter changes in untreated, early stage Parkinson's disease without dementia. *Parkinsonism Relat. Disord.* **20**, 622–626 (2014).
5. Sterling, N. W. et al. Striatal shape in Parkinson's disease. *Neurobiol. Aging* **34**, 2510–2516 (2013).
6. Rahayel, S. et al. Brain atrophy in Parkinson's disease with polysomnography-confirmed REM sleep behavior disorder. *Sleep* **42**, zsz062 (2019).
7. Nyberg, E. M. et al. Morphologic changes in the mesolimbic pathway in Parkinson's disease motor subtypes. *Parkinsonism Relat. Disord.* **21**, 536–540 (2015).
8. Tanner, J. J., McFarland, N. R. & Price, C. C. Striatal and hippocampal atrophy in idiopathic Parkinson's disease patients without dementia: a morphometric analysis. *Front. Neurol.* **8**, 139 (2017).
9. Chung, S. J. et al. Subcortical shape analysis of progressive mild cognitive impairment in Parkinson's disease. *Mov. Disord.* **32**, 1447–1456 (2017).
10. Mak, E., Bergsland, N., Dwyer, M. G., Zivadinov, R. & Kandiah, N. Subcortical atrophy is associated with cognitive impairment in mild Parkinson disease: a combined investigation of volumetric changes, cortical thickness, and vertex-based shape analysis. *AJNR Am. J. Neuroradiol.* **35**, 2257–2264 (2014).
11. Devignes, Q. et al. Posterior cortical cognitive deficits are associated with structural brain alterations in mild cognitive impairment in Parkinson's disease. *Front. Aging Neurosci.* <https://doi.org/10.3389/fnagi.2021.668559> (2021).
12. Garg, A., Appel-Cresswell, S., Popuri, K., McKeown, M. J. & Beg, M. F. Morphological alterations in the caudate, putamen, pallidum, and thalamus in Parkinson's disease. *Front. Neurosci.* **9**, 101 (2015).
13. Baggio, H. C. et al. Resting-state frontostriatal functional connectivity in Parkinson's disease-related apathy. *Mov. Disord.* **30**, 671–679 (2015).
14. Caligiuri, M. E. et al. Alterations of putaminal shape in de novo Parkinson's disease. *Mov. Disord.* **31**, 676–683 (2016).
15. D'Cruz, N. et al. Thalamic morphology predicts the onset of freezing of gait in Parkinson's disease. *NPJ Parkinsons Dis.* **7**, 20 (2021).
16. Gazzina, S. et al. Subcortical matter in the α -synucleinopathies spectrum: an MRI pilot study. *J. Neurol.* **263**, 1575–1582 (2016).
17. Gong, L. et al. Striatum shape hypertrophy in early stage Parkinson's disease with excessive daytime sleepiness. *Front. Neurosci.* **13**, 1353 (2019).
18. Hopes, L. et al. Magnetic resonance imaging features of the nigrostriatal system: Biomarkers of Parkinson's disease stages? *PLoS One* **11**, e0147947 (2016).
19. McKeown, M. J. et al. Shape (but not volume) changes in the thalamus in Parkinson disease. *BMC Neurol.* **8**, 8 (2008).
20. Peralta, M., Baxter, J. S. H., Khan, A. R., Haegelen, C. & Jannin, P. Striatal shape alteration as a staging biomarker for Parkinson's disease. *Neuroimage Clin.* <https://doi.org/10.1016/j.nicl.2020.102272> (2020).
21. Prashanth, R., Roy, S. D., Mandal, P. K. & Ghosh, S. High-accuracy classification of Parkinson's disease through shape analysis and surface fitting in 123I-lobflupane SPECT imaging. *IEEE J. Biomed. Health Inf.* **21**, 794–802 (2017).

22. de Schipper, L. J. et al. Regional structural hippocampal differences between dementia with Lewy bodies and Parkinson's disease. *J. Parkinsons Dis.* **9**, 775–783 (2019).
23. Sigirli, D. et al. Statistical shape analysis of putamen in early-onset Parkinson's disease. *Clin. Neurol. Neurosurg.* **209**, 106936 (2021).
24. Sivaranjini, S. & Sujatha, C. M. Morphological analysis of subcortical structures for assessment of cognitive dysfunction in Parkinson's disease using multi-atlas based segmentation. *Cogn. Neurodyn.* **15**, 835–845 (2021).
25. Vervoort, G. et al. Structural brain alterations in motor subtypes of Parkinson's disease: evidence from probabilistic tractography and shape analysis. *PLoS One* **11**, e0157743 (2016).
26. Varoquaux, G. & Cheplygina, V. Machine learning for medical imaging: methodological failures and recommendations for the future. *NPJ Digit Med.* **5**, 48 (2022).
27. Laansma, M. A. et al. International multicenter analysis of brain structure across clinical stages of Parkinson's disease. *Mov. Disord.* **36**, 2583–2594 (2021).
28. Zhao, Y. J. et al. Progression of Parkinson's disease as evaluated by Hoehn and Yahr stage transition times. *Mov. Disord.* **25**, 710–716 (2010).
29. Sarasso, E., Agosta, F., Piramide, N. & Filippi, M. Progression of grey and white matter brain damage in Parkinson's disease: a critical review of structural MRI literature. *J. Neurol.* **268**, 3144–3179 (2021).
30. Chung, S. J. et al. Patterns of striatal dopamine depletion in early Parkinson's disease: prognostic relevance. *Neurology* **95**, e280–e290 (2020).
31. Oh, M. et al. Subregional patterns of preferential striatal dopamine transporter loss differ in Parkinson's disease, progressive supranuclear palsy, and multiple-system atrophy. *J. Nucl. Med.* **53**, 399–406 (2012).
32. Kish, S. J., Shannak, K. & Hornykiewicz, O. Uneven pattern of dopamine loss in the striatum of patients with idiopathic Parkinson's disease. Pathophysiologic and clinical implications. *N. Engl. J. Med.* **318**, 876–880 (1988).
33. Hornykiewicz, O. Biochemical aspects of Parkinson's disease. *Neurology* **51**, S2–S9 (1998).
34. Braak, H., Ghebremedhin, E., Rüb, U., Bratzke, H. & Del Tredici, K. Stages in the development of Parkinson's disease-related pathology. *Cell Tissue Res.* **318**, 121–134 (2004).
35. Hely, M. A., Reid, W. G. J., Adena, M. A., Halliday, G. M. & Morris, J. G. L. The Sydney multicenter study of Parkinson's disease: the inevitability of dementia at 20 years. *Mov. Disord.* **23**, 837–844 (2008).
36. Aarsland, D. et al. Cognitive decline in Parkinson's disease. *Nat. Rev. Neurol.* **13**, 217–231 (2017).
37. Aarsland, D. et al. Parkinson's disease-associated cognitive impairment. *Nat. Rev. Dis. Prim.* **7**, 47 (2021).
38. Jia, X. et al. Longitudinal study of gray matter changes in Parkinson's disease. *AJNR Am. J. Neuroradiol.* **36**, 2219–2226 (2015).
39. Helmich, R. C., Janssen, M. J. R., Oyen, W. J. G., Bloem, B. R. & Toni, I. Pallidal dysfunction drives a cerebellothalamic circuit into Parkinson's tremor. *Ann. Neurol.* **69**, 269–281 (2011).
40. Owens-Walton, C. et al. Increased functional connectivity of thalamic subdivisions in patients with Parkinson's disease. *PLoS One* **14**, e0222002 (2019).
41. Dong, J., Hawes, S., Wu, J., Le, W. & Cai, H. Connectivity and functionality of the globus pallidus externa under normal conditions and Parkinson's disease. *Front. Neural Circuits* **15**, 645287 (2021).
42. Ingham, C. A., Hood, S. H., Mijster, M. J., Baldock, R. A. & Arbutnot, G. W. Plasticity of striatopallidal terminals following unilateral lesion of the dopaminergic nigrostriatal pathway: a morphological study. *Exp. Brain Res.* **116**, 39–49 (1997).
43. Charroud, C. & Turella, L. Subcortical grey matter changes associated with motor symptoms evaluated by the Unified Parkinson's disease Rating Scale (part III): A longitudinal study in Parkinson's disease. *Neuroimage Clin.* **31**, 102745 (2021).
44. García-Cabezas, M. A., Rico, B., Sánchez-González, M. A. & Cavada, C. Distribution of the dopamine innervation in the macaque and human thalamus. *Neuroimage* **34**, 965–984 (2007).
45. Halliday, G. M. Thalamic changes in Parkinson's disease. *Parkinsonism Relat. Disord.* **15**, S152–S155 (2009).
46. Rüb, U., Del Tredici, K., Schultz, C. & Ghebremedhin, E. Parkinson's disease: the thalamic components of the limbic loop are severely impaired by α -synuclein immunopositive inclusion body pathology. *Neurobiol. Aging* **23**, 245–254 (2002).
47. Haufe, S. et al. On the interpretation of weight vectors of linear models in multivariate neuroimaging. *Neuroimage* **87**, 96–110 (2014).
48. Nandhagopal, R. et al. Longitudinal progression of sporadic Parkinson's disease: a multi-tracer positron emission tomography study. *Brain* **132**, 2970–2979 (2009).
49. Hoehn, M. M. & Yahr, M. D. Parkinsonism: onset, progression and mortality. *Neurology* **17**, 427–442 (1967).
50. Nasreddine, Z. S. et al. The Montreal cognitive assessment, MoCA: a brief screening tool for mild cognitive impairment. *J. Am. Geriatr. Soc.* **53**, 695–699 (2005).
51. Fahn, S. Unified Parkinson's disease rating scale. *Recent Dev. Parkinson's Dis.* **0**, 153–163 (1987).
52. Goetz, C. G. et al. Movement Disorder Society-sponsored revision of the unified Parkinson's disease rating scale (MDS-UPDRS): scale presentation and clinimetric testing results. *Mov. Disord.* **23**, 2129–2170 (2008).
53. Daniel, H., Kosuke, I., Gary, K. & Elizabeth, A.S. MatchIt: nonparametric preprocessing for parametric causal inference. *J. Stat. Softw.* <https://doi.org/10.18637/jss.v042.i08> (2011)
54. Dale, A. M., Fischl, B. & Sereno, M. I. Cortical surface-based analysis. I. Segmentation and surface reconstruction. *Neuroimage* **9**, 179–194 (1999).
55. Ségonne, F. et al. A hybrid approach to the skull stripping problem in MRI. *Neuroimage* **22**, 1060–1075 (2004).
56. Fischl, B., Sereno, M. I. & Dale, A. M. Cortical surface-based analysis. II: inflation, flattening, and a surface-based coordinate system. *Neuroimage* **9**, 195–207 (1999).
57. Fischl, B., Liu, A. & Dale, A. M. Automated manifold surgery: constructing geometrically accurate and topologically correct models of the human cerebral cortex. *IEEE Trans. Med. Imaging* **20**, 70–80 (2001).
58. Ségonne, F., Pacheco, J. & Fischl, B. Geometrically accurate topology-correction of cortical surfaces using nonseparating loops. *IEEE Trans. Med. Imaging* **26**, 518–529 (2007).
59. Fischl, B., Sereno, M. I., Tootell, R. B. & Dale, A. M. High-resolution intersubject averaging and a coordinate system for the cortical surface. *Hum. Brain Mapp.* **8**, 272–284 (1999).
60. Gutman, B. A., Wang, Y., Rajagopalan, P., Toga, A. W. & Thompson, P. M. Shape matching with medial curves and 1-D group-wise registration. In *2012 9th IEEE International Symposium on Biomedical Imaging (ISBI)* 716–719 (IEEE, 2012).
61. Gutman, B. A., Madsen, S. K., Toga, A. W. & Thompson, P. M. A Family of fast spherical registration algorithms for cortical shapes. In *Multimodal Brain Image Analysis* 246–257 (Springer International Publishing, 2013).
62. Gutman, B. A. et al. Medial demons registration localizes the degree of genetic influence over subcortical shape variability: an $N = 1480$ meta-analysis. *Proc. IEEE Int. Symp. Biomed. Imaging* **2015**, 1402–1406 (2015).
63. Bates, D., Mächler, M., Bolker, B. & Walker, S. Fitting linear mixed-effects models using lme4. *J. Stat. Softw.* **67**, 1–48 (2015).
64. Goetz, C. G., Stebbins, G. T. & Tilley, B. C. Calibration of unified Parkinson's disease rating scale scores to Movement Disorder

- Society-unified Parkinson's disease rating scale scores. *Mov. Disord.* **27**, 1239–1242 (2012).
65. Gutman, B. A. et al. A meta-analysis of deep brain structural shape and asymmetry abnormalities in 2,833 individuals with schizophrenia compared with 3,929 healthy volunteers via the ENIGMA Consortium. *Hum. Brain Mapp.* **43**, 352–372 (2022).
 66. Alexander-Bloch, A. F. et al. On testing for spatial correspondence between maps of human brain structure and function. *Neuroimage* **178**, 540–551 (2018).
 67. Dohmatob, E. D., Gramfort, A., Thirion, B. & Varoquaux, G. Benchmarking solvers for TV- ℓ_1 least-squares and logistic regression in brain imaging. *2014 International Workshop on Pattern Recognition in Neuroimaging* (PRNI, Tübingen, 2014); <https://doi.org/10.1109/pmi.2014.6858516>.
 68. Nir, T. M. et al. Alzheimer's disease classification with novel microstructural metrics from diffusion-weighted MRI. In *Computational Diffusion MRI* 41–54 (Springer International Publishing, Cham, 2016).
 69. de Pierrefeu, A. et al. Structured sparse principal components analysis with the TV-elastic net penalty. *IEEE Trans. Med. Imaging* **37**, 396–407 (2018)

Acknowledgements

We thank all the students and research assistants for their contribution to the data collection and analysis, in particular Riccardo Galli, Mathijs Harmsen, Mahdiah Vahdatian, and Anjani Ragothaman. We thank Sophia Thomopoulos for her continuous administrative support and for creating the ENIGMA-PD cohort world map. In memoriam: Gianfranco Spalletta (8/8/1962–18/3/2023). ENIGMA core: this work was supported in part by NIH grants R01NS107513, R56AG058854, R01AG059874, R01MH116147, R01MH117601, and U54EB020403, the Michael J. Fox Foundation grant 14848 and 021683, and the Kavli Foundation Neurodata Without Borders. PPMI—data used in the preparation of this article were obtained from the Parkinson's Progression Markers Initiative (PPMI) database (www.ppmi-info.org/access-data-specimens/download-data). For up-to-date information on the study, visit www.ppmi-info.org. PPMI—a public-private partnership—is funded by the Michael J. Fox Foundation for Parkinson's Research and funding partners, including 4D Pharma, AbbVie, AcureX Therapeutics, Allergan, Amathus Therapeutics, Aligning Science Across Parkinson's (ASAP), Avid Radiopharmaceuticals, Bial Biotech, Biogen, BioLegend, Bristol-Myers Squibb, Celgene Corporation, DaCapo Brainscience, Denali Therapeutics, The Edmond J. Safra Foundation, Eli Lilly and Company, GE Healthcare, GlaxoSmithKline, Golub Capital, Handl Therapeutics, Insitro, Janssen Pharmaceuticals, Lundbeck, Merck & Co., Inc., Meso Scale Diagnostics (MSD), LLC, Neurocrine Biosciences, Pfizer Inc., Piramal Imaging, Prevail Therapeutics, F. Hoffmann-La Roche Ltd and its affiliated company Genentech Inc., Sanofi Genzyme, Servier, Takeda Pharmaceutical Company, Teva Neuroscience, Inc., UCB, Vanqua Bio, Verily Life Sciences, Voyager Therapeutics, Inc., and Yumanity Therapeutics, Inc. OpenNeuro Japan cohort—these data were obtained from the OpenfMRI database. Its accession number is ds000245. This research was supported in part by the following: a grant-in-aid from the Research Committee of Central Nervous System Degenerative Diseases by the Ministry of Health, Labor, and Welfare, Integrated Research on Neuropsychiatric Disorders project, carried out by SRBPS; a Grant-in-Aid for Scientific Research on Innovative Areas (Brain Protein Aging and Dementia Control 26117002) from the MEXT of Japan; Integrated Research on Neuropsychiatric Disorders carried out under the Strategic Research Program for Brain Sciences, Scientific Research on Innovative Areas (Comprehensive Brain Science Network); and Integrated Research on Depression, Dementia, and Development Disorders by the Strategic Research Program for Brain Sciences from the Japan Agency for Medical Research and Development (AMED). NEUROCON cohort—this work was partially supported by the NEUROCON project (84/2012), financed by UEFISCDI. Amsterdam I and III cohort—grant support (not for this study) from the Netherlands Organization for Health

Research and Development, the Michael J. Fox Foundation, and the Hersenstichting. Amsterdam II (Cogtips) cohort—Cogtips is supported by the Dutch Parkinson's Disease Association (“Parkinson Vereniging” 19–2015) and Brain Foundation of the Netherlands (“Hersenstichting” HA-2017-00227). Liege I & II cohorts—this work was funded by PDR Grant T0.165.14, National Fund for Scientific Research (FNRS), Belgium. Donders cohort—this work was funded by a grant of the Dutch Brain Foundation (grant F2013(10–15 to R.H.), from the Netherlands Organization for Scientific Research (VENI grant 91617077, VIDI grant 09150172010044), and from the Michael J. Fox Foundation. Rome SLF cohort—this work was funded by the Italian Ministry of Health, Italian Ministry of Health RC12-13-14-15-16-17-18-19/A. UNICAMP cohort—this work was funded by the São Paulo Research Foundation FAPESP-BRAINN (2013–07559-3). Christchurch cohort—This work was supported by the Health Research Council of New Zealand, Canterbury Medical Research Foundation, Neurological Foundation of New Zealand, University of Otago Research Grant, and Brain Research New Zealand. Charlottesville I–III cohorts—this work was supported by grants from the Department of Defense, Commonwealth of Virginia's Alzheimer's and Related Diseases Research Award Fund, and the University of Virginia. Manchester I and II cohorts—this work was funded by the Sydney Driscoll Neuroscience Foundation, Lancaster University and the Sir John Fisher Foundation, University of Manchester Biomedical Imaging Institute, Medical Research Council UK Doctoral Training Program, Engineering and Physical Science Research Council UK (EP/M005909/1). Pennsylvania cohort—this work was funded by the NINDS, NIH AG062418 (U19), and NS053488 (P50). Chang Gung cohort—this work was supported by MOST 106-2314-B-182-018-MY3, EMRPD1K0451, EMRPD1K0481. UDALL—this work was funded by NIH grants RC4 NS073008 and P50 NS062684, and Ruth L. Kirschstein National Research Service Award T32AG0000258. Data paper: <https://doi.org/10.1089/brain.2014.0248>. Stanford I and II cohorts—funded by NIH/NINDS NS075097, NS115114, and the Michael J Fox Foundation. T.J.A. is funded by Health Research Council grants (20/538, 21/165). H.W.B. is funded by ZonMw, Michael J Fox Foundation. F.C. is funded by FAPESP grant 2013/07559-3. M.D. is funded by a grant from ParkinsonNL (P2023-14). H.E. is funded by EPSRC UK. J.D. is funded by an ENIGMA-PD R01 grant. J.C.D.A. is funded by the Health Research Council of New Zealand (20/538); Marsden Fund New Zealand (UOC2105); Neurological Foundation of New Zealand (2232 PRG) and the Research and Education Trust Pacific Radiology (MRIJDA). G.G. is funded by an FNRS grant (Belgian Fund for Scientific Research; University of Liege Liege Grant(Fonds Rahier). R.C.H. is funded by the MJ Fox Foundation and the Netherlands Organization for Scientific Research. N.J. is funded by grants R01AG059874, R01MH117601, R01NS107513, R01AG058854, and P41EB015922. C.M. is funded by NIH R01 grants NIH R01AG066152; NIH P01AG066597; NIH U54NS092091; NIH. U01NS107027; NIH R01NS109260; NIH U19AG062418; PA Dept of Health 2019NF4100087335; NIH R01 AG070885; NIH P30AG072979; NIH R01NS107513; NIH R01 AG076832; and NIH R01AG080734. T.M. is funded by a Health Research Council grant (20/538). K.P. is funded by the Michael J Fox Foundation for Parkinson's Research, the Lewy Body Dementia Association, the Alzheimer's Drug Discovery Foundation, and the NIH. F.P. is funded by the Italian Ministry of Health, grant number RF-2019-12370182. C.R. is funded by SNF grants #204593 and #180365. D.J.S. is funded by the SAMRC. C.Y. is funded by the NIH, Alzheimer's Association, and New Vision Research. L.M.P. is funded by EPSRC UK, MRC UK, GE Medical Systems, and the Academy of Medical Sciences, UK. T.P. is funded by a Health Research Council grant (21/165). O.A.v.d.H. is funded by NWO/ZonMw, Hersenstichting, and the NIMH. C.V. is funded by the Michael J Fox Foundation. D.V. is funded by the Italian Ministry of Health, Ricerca Corrente 2023. J.W. is funded by the National Science and Technology Council, Taiwan. R.W. is funded by SNF grant #180365. C.Y. is funded by São Paulo Research Foundation FAPESP-BRAINN Grant # 2013–07559-3; CNPQ (#315953/2021-7) National Council for Scientific and Technological Development. P.M.T. is funded by grants from the NIH. B.A.G. is funded by grants from the Alzheimer's Association 2018–AARG-592081 and Michael J Fox

Foundation MJFF-021683. D.W. is funded by grants from NIA U19 AG062418. Y.Z. is funded by grants from the Alzheimer's Association 2018-AARG-592081 and the Michael J Fox Foundation MJFF-021683. Y.D.v.d.W. is funded by NINDS Award 1R01NS107513-01A1 and NIA Award 1R01AG058854-01A1.

Author contributions

M.A.L., Y.Z., and E.M.v.H. contributed equally and shared co-first authorship. All authors meet the following four criteria: (1) they contributed substantially to the conception or design of the work, or the acquisition, analysis, or interpretation of data; (2) they participated in drafting or revising the manuscript for important intellectual content; (3) they have given final approval of the version to be published; and (4) they agree to be accountable for all aspects of the work, ensuring that any questions related to the accuracy or integrity of any part of the study are appropriately investigated and resolved. Below is a detailed description of the specific contributions made by each author to various aspects of the study. 1. Research project: A. conception, B. organization, and C. execution; 2. Statistical analysis: A. design, B. execution, and C. review and critique; and 3. Manuscript preparation: A. writing of the first draft and B. review and critique. M.A.L.: 1A–C, 2A, 2B, and 3A. Y.Z.: 1A–C, 2A, 2B, and 3A. E.M.v.H.: 1A–C, 2A, 2B, and 3A. J.K.B.: 1A–C, 2A, and 3B. C.O.W.: 1B, 1C, 2C, and 3B. S.A.B.: 1C, 2C, and 3B. T.J.A.: 1C, 2C, and 3B. F.A.: 1C, 2C, and 3B. H.W.B.: 1C, 2C, and 3B. F.C.: 1C, 2C, and 3B. J.C.D.A.: 1C, 2C, and 3B. M.F.D.: 1C, 2C, and 3B. JD: 1C, 2C, and 3B. H.C.A.E.: 1C, 2C, and 3B. G.G.: 1C, 2C, and 3B. R.C.H.: 1A, 1C, 2A, 2C, and 3B. C.L.: 1C, 2C, and 3B. C.T.M.: 1C, 2C, and 3B. T.R.M.: 1C, 2C, and 3B. B.N.: 1C, 2C, and 3B. L.M.P.: 1C, 2C, and 3B. C.P.: 1C, 2C, and 3B. F.P.: 1C, 2C, and 3B. T.L.P.: 1C, 2C, and 3B. K.L.P.: 1C, 2C, and 3B. M.R.: 1C, 2C, and 3B. C.R.: 1C, 2C, and 3B. R.S.: 1C, 2C, and 3B. P.S.: 1C, 2C, and 3B. L.S.: 1C, 2C, and 3B. D.J.S.: 1C, 2C, and 3B. T.D.v.B.: 1C, 2C, and 3B. O.a.v.d.H.: 1C, 2C, and 3B. D.V.: 1C, 2C, and 3B. C.V.: 1C, 2C, and 3B. J.W.: 1C, 2C, and 3B. R.W.: 1C, 2C, and 3B. C.L.Y.: 1C, 2C, and 3B. I.D.: 1C, 2C, and 3B. J.P.F.: 1C, 2C, and 3B. R.P.G.: 1C, 2C, and 3B. M.H.: 1C, 2C, and 3B. D.I.: 1C, 2A, 2C, and 3B. H.B.K.: 1C, 2C, and 3B. J.C.K.: 1C, 2C, and 3B. L.F.R.: 1C, 2C, and 3B. C.S.R.: 1C, 2C, and 3B. L.S.R.S.: 1C, 2C, and 3B. D.W.: 1C, 2C, and 3B. N.J.: 1A, 2C, and 3B. P.M.T.: 1A, 2C, and 3B. Y.D.v.d.W.: 1A, 1B, 2A, 2C, and 3B. B.A.G.: 1A, 1B, 2A, 2C, and 3B.

Competing interests

The authors declare no competing interests related to this article. B.A.G. provides consulting services for Natera, Inc. D.J.S. has received consultancy honoraria in the past 3 years from Discovery Vitality, Johnson & Johnson,

Kanna, L'Oreal, Lundbeck, Orion, Sanofi, Servier, Takeda, and Vistagen. P.S. reports personal fees from Bial, AbbVie, and Boston Scientific. G.G. owns stocks in Koios Care (<https://www.koios.care/>) and has received consultancy fees from Abbvie Belgium, Zambon Belgium, and EG Belgium (Stada group). He also received an Honorarium from Abbvie Belgium, Zambon Belgium, and EG Belgium. J.W. has received Honoraria from the Movement Disorders Society. K.P. owns stocks in Amprion and Curasen. She has also received honoraria from invited scientific presentations to universities and professional societies not exceeding \$5000/yr and provides consulting services to Curasen. J.K. has received Honoraria from Ipsen and Merz. Y.D.v.d.W. has received a speaker's fee for postdoctoral training organized by Medilex and AbbVie.

Additional information

Supplementary information The online version contains supplementary material available at <https://doi.org/10.1038/s41531-024-00825-9>.

Correspondence and requests for materials should be addressed to Max A. Laansma.

Reprints and permissions information is available at <http://www.nature.com/reprints>

Publisher's note Springer Nature remains neutral with regard to jurisdictional claims in published maps and institutional affiliations.

Open Access This article is licensed under a Creative Commons Attribution 4.0 International License, which permits use, sharing, adaptation, distribution and reproduction in any medium or format, as long as you give appropriate credit to the original author(s) and the source, provide a link to the Creative Commons licence, and indicate if changes were made. The images or other third party material in this article are included in the article's Creative Commons licence, unless indicated otherwise in a credit line to the material. If material is not included in the article's Creative Commons licence and your intended use is not permitted by statutory regulation or exceeds the permitted use, you will need to obtain permission directly from the copyright holder. To view a copy of this licence, visit <http://creativecommons.org/licenses/by/4.0/>.

© The Author(s) 2024

¹Amsterdam UMC, Department of Anatomy and Neurosciences, Vrije Universiteit Amsterdam, Amsterdam, The Netherlands. ²Amsterdam Neuroscience, Neurodegeneration, Amsterdam, The Netherlands. ³Department of Biomedical Engineering, Illinois Institute of Technology, Chicago, IL, USA. ⁴Social, Genetic and Developmental Psychiatry Centre, Institute of Psychiatry, Psychology and Neuroscience, King's College London, London, UK. ⁵Imaging Genetics Center, Mark and Mary Stevens Neuroimaging and Informatics Institute, Keck School of Medicine, University of Southern California, Marina del Rey, CA, USA. ⁶Faculty of Health and Medicine, The University of Lancaster, Lancaster, UK. ⁷Department of Neurology, Royal Preston Hospital, Preston, UK. ⁸Department of Medicine, University of Otago, Christchurch, Christchurch, New Zealand. ⁹New Zealand Brain Research Institute, Christchurch, New Zealand. ¹⁰Neurology Department, Te Wahtu Ora—Health New Zealand Waitaha Canterbury, Christchurch, New Zealand. ¹¹Laboratory of Neuropsychiatry, IRCCS Santa Lucia Foundation, Rome, Italy. ¹²Amsterdam UMC, Department Psychiatry, Vrije Universiteit Amsterdam, Amsterdam, The Netherlands. ¹³Amsterdam UMC, Department Neurology, Vrije Universiteit Amsterdam, Amsterdam, The Netherlands. ¹⁴Department of Neurology, University of Campinas—UNICAMP, Campinas, Brazil. ¹⁵Brazilian Institute of Neuroscience and Neurotechnology, Campinas, Brazil. ¹⁶School of Psychology, Speech and Hearing, University of Canterbury, Christchurch, New Zealand. ¹⁷Department of Neurology, Inselspital, University of Bern, Bern, Switzerland. ¹⁸Department of Neurology and Center of Expertise for Parkinson & Movement Disorders, Donders Institute for Brain, Cognition and Behaviour, Radboud University Nijmegen Medical Centre, Nijmegen, The Netherlands. ¹⁹Department of Radiology and Medical Imaging, University of Virginia, Charlottesville, VA, USA. ²⁰Lancaster Medical School, Lancaster University, Lancaster, UK. ²¹Division of Neuroscience and Experimental Psychology, Faculty of Biology, Medicine and Health, The University of Manchester, Manchester Academic Health Science Centre, Manchester, UK. ²²Department of Psychiatry and Mental Health, University of Cape Town, Cape Town, South Africa. ²³GIGA-CRC in vivo imaging, University of Liège, Liège, Belgium. ²⁴Department of Neurology, CHU Liège, Liège, Belgium. ²⁵Department of Neurology and Center of Expertise for Parkinson & Movement Disorders, Donders Institute for Brain, Cognition and Behaviour, Radboud University Medical Centre, Nijmegen, The Netherlands. ²⁶Centre for Cognitive Neuroimaging, Donders Institute for Brain, Cognition and Behaviour, Radboud University Nijmegen, Nijmegen, The Netherlands. ²⁷Division of Clinical Neurology, Department of Clinical Neurosciences, Oxford Parkinson's Disease Centre, Nuffield, University of Oxford, Oxford, UK. ²⁸Department of Biomedical Engineering, Duke University, Durham, NC, USA. ²⁹Department of Neurology & Neurological Sciences, Stanford University, Palo Alto, CA, USA. ³⁰SA MRC Unit on Risk and Resilience in Mental Disorders, Department of Psychiatry, Stellenbosch University, Cape

Town, South Africa. ³¹University of Pennsylvania Perelman School of Medicine, Philadelphia, PA, USA. ³²Division of Psychology, Communication and Human Neuroscience, School of Health Sciences, Faculty of Biology, Medicine and Health, The University of Manchester, Manchester, UK. ³³Geoffrey Jefferson Brain Research Centre, Manchester Academic Health Science Centre, Northern Care Alliance & University of Manchester, Manchester, UK. ³⁴Excellence Center for Advanced MR Techniques and Parkinson's Disease Center, Neurology unit, Fondazione IRCCS Cà Granda Maggiore Policlinico Hospital, University of Milan, Milan, Italy. ³⁵Department of Neurosciences, Neurology Unit, Fondazione Ca' Granda, IRCCS, Ospedale Policlinico, University of Milan, Milano, Italy. ³⁶Support Center for Advanced Neuroimaging, (SCAN) University Institute of Diagnostic and Interventional Neuroradiology, Inselspital, Bern University Hospital, University of Bern, Bern, Switzerland. ³⁷Department of Neurology, Medical University of Graz, Graz, Austria. ³⁸Department of Pathophysiology and Transplantation, University of Milan, Milan, Italy. ³⁹SA MRC Unit on Risk & Resilience in Mental Disorders, Department of Psychiatry and Neuroscience Institute, University of Cape Town, Cape Town, South Africa. ⁴⁰Amsterdam Neuroscience, Brain Imaging, Amsterdam, The Netherlands. ⁴¹Department of Medical Imaging and Radiological Sciences, Chang Gung University, Taoyuan City, Taiwan. ⁴²Department of Diagnostic Radiology, Chang Gung Memorial Hospital, Keelung Branch, Keelung City, Taiwan. ⁴³Healthy Ageing Research Center, Chang Gung University, Taoyuan City, Taiwan. ⁴⁴Support Center for Advanced Neuroimaging (SCAN), University Institute of Diagnostic and Interventional Neuroradiology, University Hospital Bern, Bern, Switzerland. ⁴⁵These authors contributed equally: Max A. Laansma, Yuji Zhao, Eva M. van Heese.

✉ e-mail: m.laansma@amsterdamumc.nl